

A Zeroth-Order Block Coordinate Descent Algorithm for Huge-Scale Black-Box Optimization

HanQin Cai¹, Yuchen Lou², Daniel McKenzie¹, and Wotao Yin³

¹University of California, Los Angeles,
Los Angeles, CA, USA

²The University of Hong Kong,
Pokfulam, Hong Kong, PRC

³Damo Academy,
Alibaba US,
Bellevue, WA, USA

February 28, 2025

Abstract

We consider the zeroth-order optimization problem in the huge-scale setting, where the dimension of the problem is so large that performing even basic vector operations on the decision variables is infeasible. In this paper, we propose a novel algorithm, coined ZO-BCD, that exhibits favorable overall query complexity *and* has a much smaller per-iteration computational complexity. In addition, we discuss how the memory footprint of ZO-BCD can be reduced even further by the clever use of circulant measurement matrices. As an application of our new method, we propose the idea of crafting adversarial attacks on neural network based classifiers in a *wavelet domain*, which can result in problem dimensions of over 1.7 million. In particular, we show that crafting adversarial examples to audio classifiers in a wavelet domain can achieve the state-of-the-art attack success rate of 97.9%.

1 Introduction

We are interested in problem (1) under the restrictive assumption that one only has noisy zeroth-order access to $f(x)$ (*i.e.* one cannot access the gradient, $\nabla f(x)$) *and* the dimension

Email addresses: hqcai@math.ucla.edu (H.Q. Cai), mckenzie@math.ucla.edu (D. McKenzie), u3544766@connect.hku.hk (Y. Lou), and wotao.yin@alibaba-inc.com (W. Yin).

of the problem, d , is huge, say $d > 10^7$.

$$\underset{x \in \mathbb{R}^d}{\text{minimize}} f(x). \quad (1)$$

Such problems (with small or large d) arise frequently in domains as diverse as simulation-based optimization in chemistry and physics [1], hyperparameter tuning for combinatorial optimization solvers [2], and for neural networks [3] and online marketing [4]. Lately, algorithms for zeroth-order optimization have drawn increasing attention due to their use in finding good policies in reinforcement learning [5–7] and in crafting adversarial examples given only black-box access to neural network based classifiers [8–11]. We note that in all of these applications queries (*i.e.* evaluating $f(x)$ at a chosen point) are considered expensive, thus it is desirable for zeroth-order optimization algorithms to be as *query efficient* as possible.

Unfortunately, it is known [12] that the worst case query complexity of *any* zeroth order algorithm for strongly convex $f(x)$ scales linearly with d . Clearly, this is prohibitive for huge d . Recent work has begun to side-step this issue by assuming that $f(x)$ has additional, low-dimensional, structure. For example, [11, 13, 14] assume that the gradients $\nabla f(x)$ are (approximately) s -sparse (see Assumption 5) while [15] and others assume that $f(x) = g(Ax)$ where $A : \mathbb{R}^s \rightarrow \mathbb{R}^d$ and $s \ll d$. All of these works promise a query complexity that scales linearly with the intrinsic dimension, s , and only logarithmically with the extrinsic dimension, d . However there is no free lunch here; the improved complexity of [15] requires access to *noiseless* function evaluations, the results of [14] only hold if the support of $\nabla f(x)$ is *fixed*¹ for all $x \in \mathbb{R}^d$ and while [13] and [11] allow for noisy function evaluations and changing gradient support, both solve a computationally intensive optimization problem as a sub-routine, requiring at least $\Omega(s d \log(d))$ memory and FLOPS per iteration.

1.1 Contributions

In this paper we provide the first zeroth-order optimization algorithm enjoying a sub-linear (in d) query complexity *and* a sub-linear per-iteration computational complexity. In addition, our algorithm has an exceptionally small memory footprint. Furthermore, it does not require the repeated sampling of d -dimensional random vectors, a hallmark of many zeroth-order optimization algorithms. With this new algorithm, ZO-BCD, in hand we are able to solve black-box optimization problems of a size hitherto unimagined. Specifically, we consider the problem of generating adversarial examples to fool neural-network-based classifiers, given only black-box access to the model (as introduced in [8]). However, we consider generating these malicious examples by perturbing natural examples *in a wavelet domain*. For image classifiers (we consider Inception-v3 trained on ImageNet) we are able to produce attacked images with a record low ℓ_2 distortion of 13.7 and a success rate of 96%, exceeding the state-of-the-art. See Figure 1.1 for an example of attacking the original image with label

¹See Appendix A of [11] for a proof of this.

“scale” to the mis-classified label “switch”, with an almost imperceptible noise. For audio classifiers, switching to a wavelet domain results in a problem dimension of over 1.7 million. Using ZO-BCD, this is not an issue and we achieve a targeted attack success rate of 97.93% with a mean distortion of -6.32 dB.

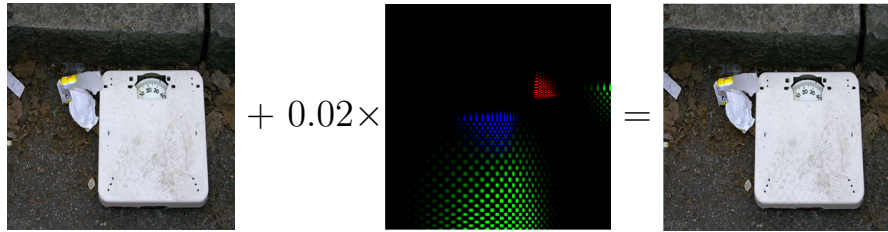


Figure 1: Wavelet attacked image by ZO-BCD: true label “scale” \rightarrow mis-classified label “switch”.

1.2 Relation to prior work

As mentioned above, the recent works [11, 13, 14] provide zeroth-order algorithms whose query complexity scales linearly with s and logarithmically with d . In order to ameliorate the prohibitive computational and memory cost associated with huge d , several domain-specific heuristics have been employed in the literature. For example in [8, 16], in relation to adversarial attacks, an upsampling operator $D : \mathbb{R}^p \rightarrow \mathbb{R}^d$ with $p \ll d$ is employed. Problem (1) is then replaced with the lower dimensional problem: $\text{minimize}_{z \in \mathbb{R}^p} f(D(z))$. Several other works [10, 11, 17] choose a low dimensional random subspace $T_k \subset \mathbb{R}^d$ at each iteration and then restrict $x_{k+1} - x_k \in T_k$. We emphasize that none of the aforementioned works *prove* that such a procedure will converge, and our work is partly motivated by the desire to provide this empirically successful trick with firm guarantees of success.

In the reinforcement learning literature it is common to evaluate the $f(x_k + z_{k,i})$ on parallel devices and then send the computed function value and the perturbation $z_{k,i}$ to a central worker, which then computes x_{k+1} . As $x \in \mathbb{R}^d$ parametrizes a neural network, d can be extremely large, and hence the communication of the $z_{k,i}$ between workers becomes a bottle neck. [5] overcomes this with a “seed sharing” trick, but again this heuristic lacks rigorous analysis. We hope that ZO-BCD’s (particularly the ZO-BCD-RC variant, see Section 3) intrinsically small memory footprint will make it a competitive, principled alternative.

Finally, although two recent works have examined the idea of wavelet domain adversarial attacks [18, 19] they are of a very different nature to our approach. We discuss this further in Section 4.

1.3 Assumptions and notation

As mentioned, we will suppose that the decision variables x have been subdivided into J blocks of sizes $d^{(1)}, \dots, d^{(J)}$. Following the notation of [20], we shall suppose that there exists a permutation matrix $U \in \mathbb{R}^{d \times d}$ and a division of U into submatrices $U = [U^{(1)}, U^{(2)}, \dots, U^{(J)}]$ such that $U^{(j)} \in \mathbb{R}^{d \times d^{(j)}}$ and that the j -th block is spanned by the columns of $U^{(j)}$. Letting $x^{(j)}$ denote the decision variables in the j -th block, we can write $x = \sum_{j=1}^J U^{(j)}x^{(j)}$ or simply $x = (x^{(1)}, x^{(2)}, \dots, x^{(J)})$ for short. We shall consistently use the notation $g(x) := \nabla f(x)$, omitting x if it is clear from context. By $g^{(j)}(x)$ we shall mean the components of the gradient corresponding to the j -th block, *i.e.* $g^{(j)}(x) = \nabla_{x^{(j)}} f(x)$. We shall think of this either a vector in \mathbb{R}^d or in $\mathbb{R}^{d^{(j)}}$. Finally, we use $\tilde{\mathcal{O}}(\cdot)$ notation to suppress logarithmic factors. Let us now introduce some standard assumptions on the objective function.

Assumption 1 (Block Lipschitz differentiability). $f(x)$ is continuously differentiable and, for any $j = 1, \dots, J$, any $x \in \mathbb{R}^d$ and any $t \in \mathbb{R}^{d^{(j)}}$ we have that:

$$\|g^{(j)}(x) - g^{(j)}(x + U^{(j)}t)\|_2 \leq L_j \|t\|_2$$

for some fixed constant L_j .

One can easily check that if $f(x)$ is L -Lipschitz differentiable then it is also block Lipschitz differentiable, with $\max_j L_j \leq L$.

Assumption 2 (Convexity). For any $x, y \in \mathbb{R}^d$, $t \in [0, 1]$, we have that $f(tx + (1 - t)y) \leq t f(x) + (1 - t)f(y)$.

Define the solution set $\mathcal{X}^* = \operatorname{argmin}_{x \in \mathbb{R}^d} f(x)$. If this set is non-empty we may define the level set radius for $x \in \mathbb{R}^d$ as:

$$\mathcal{R}(x) := \max_{y \in \mathbb{R}^d} \max_{x^* \in \mathcal{X}^*} \{\|y - x^*\|_2 : f(y) \leq f(x)\}. \quad (2)$$

Assumption 3 (Non-empty solution set and Bounded level sets). Assume that \mathcal{X}^* is non-empty and that $\mathcal{R}(x_0) < \infty$.

Assumption 4 (Adversarially noisy oracle). $f(x)$ is only accessible through a *noisy oracle*: $E_f(x) = f(x) + \xi$, where ξ is a random variable satisfying $|\xi| \leq \sigma$.

Assumption 5 (Sparse gradients). There exists a fixed integer $0 < s_{\text{exact}} < d$ such that for all $x \in \mathbb{R}^d$:

$$\|g(x)\|_0 := |\{i : g_i(x) \neq 0\}| \leq s_{\text{exact}}.$$

It is of interest to relax this assumption to an “approximately sparse” assumption, such as that in [11]. The issue here is that it is unclear that randomly chosen blocks (see Section 2.1) will inherit this property. We leave the analysis of this case for future work. Finally, let $\nabla_{jj}^2 f(x) \in \mathbb{R}^{d^{(j)} \times d^{(j)}}$ denote the j -th block Hessian.

Assumption 6 (Weakly sparse block Hessian). $f(x)$ is twice differentiable and, for all $j = 1, \dots, J$ and $x \in \mathbb{R}^d$, we have that $\|\nabla_{jj}^2 f(x)\|_1 \leq H_j$ for some fixed constant H_j .

Note that $\|\cdot\|_1$ represents the *element-wise* ℓ_1 -norm: $\|B\|_1 = \sum_{i,j} |B_{ij}|$.

2 Gradient estimators

Randomized (block) coordinate descent methods are an attractive alternative to full gradient methods for huge-scale problems [21]. ZO-BCD is a block coordinate method adapted to the zeroth-order setting and conceptually has three steps:

1. Choose a block, $j \in \{1, \dots, J\}$ at random.
2. Use zeroth-order queries to find an approximation, $\hat{g}_k^{(j)}$, of the true block gradient $g_k^{(j)}$.
3. Take a negative gradient step: $x_{k+1} = x_k - \alpha \hat{g}_k^{(j)}$.

We abuse notation slightly and use $\hat{g}_k^{(j)}$ to refer to both a $d^{(j)}$ dimensional vector for the block j , as well as the d dimensional vector obtained by appending the $d^{(j)}$ dimensional block with the rest to be zeros, for the gradient descent update.

In principle any scheme for constructing an estimator of g_k could be adapted for estimating $g_k^{(j)}$, as long as one is able to bound $\|g_k^{(j)} - \hat{g}_k^{(j)}\|_2$ with high probability. As we wish to exploit gradient sparsity, we choose to adapt the estimator presented in [11]. Let us now discuss how to do so. Fix a sampling radius $\delta > 0$. Suppose that the j -th block has been selected and select m *sample directions* $z_1, \dots, z_m \in \mathbb{R}^{d^{(j)}}$ from a Rademacher distribution². Consider the finite differences:

$$y_i = \frac{1}{\sqrt{m}} \frac{E_f(x + \delta U^{(j)} z_i) - E_f(x)}{\delta}. \quad (3)$$

Certainly, if g satisfies Assumption 5 then so does $g^{(j)}$. Thus, we may attempt to recover $g^{(j)}$ by solving the following sparse recovery problem:

$$\hat{g}^{(j)} = \underset{v \in \mathbb{R}^{d^{(j)}}}{\operatorname{argmin}} \|Zv - y\|_2 \quad \text{s.t. } \|v\|_0 \leq s. \quad (4)$$

We propose solving Problem (4) using CoSaMP [22], but certainly other choices are possible. We present this as Algorithm 1. Theorem 2.6 and Corollary 2.7 in [11] then guarantee that, for appropriately chosen parameters, $\hat{g}^{(j)}$ is a reliable estimator of $g^{(j)}$. For the reader's convenience we quantify this in the following theorem:

²That is, the entries of each z_i are $+1$ or -1 with equal probability

Algorithm 1 Block Gradient Estimation

Input: x : current point; j : choice of block; s : gradient sparsity level; δ : query radius; n : number of CoSaMP iterations; $\{z_i\}_{i=1}^m$: sample directions in $\mathbb{R}^{d^{(j)}}$.

for $i = 1$ **to** m **do**

$y_i \leftarrow (E_f(x + \delta U^{(j)} z_i) - E_f(x)) / (\sqrt{m} \delta)$

end for

$\mathbf{y} \leftarrow [y_1, \dots, y_m]^T$; $Z \leftarrow 1/\sqrt{m}[z_1, \dots, z_m]^T$

$\hat{g}^{(j)} \approx \operatorname{argmin}_{\|v\|_0 \leq s} \|Zv - \mathbf{y}\|_2$ by n iterations of CoSaMP

Output: $\hat{g}^{(j)}$: estimated block gradient.

Theorem 2.1. Suppose that $f(x)$ satisfies Assumptions 1, 5 and 6. Let $g^{(j)}$ be the output of Algorithm 1 with $\delta = 2\sqrt{\sigma/H_j}$, $s \geq s_{\text{exact}}$ and $m = b_1 s \log(d/J)$ Rademacher sample directions. Then with probability at least $1 - (s/d)^{b_2 s}$:

$$\|\hat{g}^{(j)} - g^{(j)}\|_2 \leq \rho^n \|g^{(j)}\|_2 + 2\tau \sqrt{\sigma H_j}. \quad (5)$$

The constants b_1 and b_2 are directly proportional; considering more sample directions results in a higher probability of recovery. In our experiments we consider $1 \leq b_1 \leq 4$. The constant ρ and τ arise from the analysis of CoSaMP. Both are inversely proportional to b_1 . For our range of b_1 , $\rho \approx 0.5$ and $\tau \approx 10$.

2.1 Almost equispars blocks using randomization

Suppose that $f(x)$ satisfies Assumption 5, so that $\|g(x)\|_0 \leq s_{\text{exact}}$ for all x . In general one cannot improve upon the bound $\|g^{(j)}(x)\|_0 \leq s_{\text{exact}}$, as it might be the case that all non-zero entries of g lie in the j -th block. However, by *randomizing* the blocks one can guarantee that, with high probability, the non-zero entries of g are *almost equally distributed* over the J blocks. We assume, for simplicity, that all blocks are equal-sized (i.e, $d^{(1)} = d^{(2)} = \dots = d^{(J)} = d/J$).

Theorem 2.2. Let U be a permutation matrix chosen uniformly at random. Then for any $x \in \mathbb{R}^d$ and any $\Delta > 0$ we have that $\|g^{(j)}(x)\|_0 \leq (1 + \Delta)s_{\text{exact}}/J$ for all j with probability at least $1 - 2J \exp\left(-\frac{\Delta^2 s_{\text{exact}}}{3J}\right)$.

It will be convenient to fix a value of Δ , say $\Delta = 0.1$. An immediate consequence of Theorem 2.2 is that one can significantly improve upon the query complexity of Theorem 2.1:

Corollary 2.3. Suppose that U is chosen uniformly at random. The error bound (5) in Theorem 2.1 still holds, now with probability $1 - \mathcal{O}(J \exp(-s_{\text{exact}}/J))$, if we change the assumption $s \geq s_{\text{exact}}$ to $s \geq 1.1s_{\text{exact}}/J$ (and keep all other parameters the same).

Note that this allows us to use approximately J times fewer queries per iteration.

2.2 Further reducing the required randomness

As discussed in [11], one favorable feature of using a compressed sensing based gradient estimator is that the error bound (5) is *universal*. That is, it holds for all $x \in \mathbb{R}^d$ for the *same set of sample directions* $\{z_i\}_{i=1}^m \subset \mathbb{R}^{d/J}$. This means that, instead of resampling new vectors at each iteration we may use *the same sampling directions for each block and each iteration*. Thus, only $md/J = \tilde{\mathcal{O}}(sd/J^2)$ binary random variables need to be sampled, stored and transmitted in ZO-BCD. Remarkably, one can do even better by choosing as sample directions a subset of the rows of a circulant matrix. Recall that a circulant matrix of size $d/J \times d/J$, generated by $v \in \mathbb{R}^{d/J}$, has the following form:

$$\mathcal{C}(v) = \begin{pmatrix} v_1 & v_2 & \cdots & v_{d/J} \\ v_{d/J} & v_1 & \cdots & v_{d/J-1} \\ \vdots & \ddots & \ddots & \vdots \\ v_2 & \cdots & v_{d/J} & v_1 \end{pmatrix}. \quad (6)$$

Equivalently, $\mathcal{C}(v)$ is the matrix with rows $\mathcal{C}_i(v)$ where:

$$\mathcal{C}_i(v) \in \mathbb{R}^{d/J} \quad \text{and} \quad \mathcal{C}_i(v)_j = v_{i+j-1}.$$

By exploiting recent results in signal processing, we show:

Theorem 2.4. *Assign blocks randomly as in Corollary 2.3. Let $z \in \mathbb{R}^{d/J}$ be a Rademacher random vector. Choose a random subset $\Omega = \{j_1, \dots, j_m\} \subset \{1, \dots, d/J\}$ of cardinality $m = b_3(s/J) \log^2(s/J) \log^2(d/J)$. The error bound (5) in Theorem 2.1 still holds, again with probability $1 - \mathcal{O}(J \exp(-s_{\text{exact}}/J))$, if we change $s \geq s_{\text{exact}}$ to $s \geq 1.1s_{\text{exact}}/J$ and use $z_i = \mathcal{C}_{j_i}(z)$ for all $i = 1, \dots, m$ (and keep all other parameters the same).*

This theorem implies that one only needs d/J binary random variables (to construct z) and $m = \tilde{\mathcal{O}}(s/J)$ randomly selected integers for the *entire* algorithm. Note that (partial) circulant matrices allow for a *fast multiplication*, further reducing the computational complexity of Algorithm 1.

3 The proposed algorithm: ZO-BCD

Let us now introduce our new algorithm. We consider two variants, distinguished by the kind of sampling directions used. ZO-BCD-R uses **Rademacher** sampling directions. ZO-BCD-RC uses **Rademacher-Circulant** sampling directions, as described in Section 2.2. For simplicity, we present our algorithm for randomly selected, equally sized coordinate blocks. With minor modifications our results still hold for user-defined and/or unequally sized blocks, and we discuss this in Appendix B. The following theorem guarantees that both variants converge at a sublinear rate to within a certain error tolerance. As the choice of block in each iteration is random, our results are necessarily probabilistic.

Algorithm 2 ZO-BCD

Input: x_0 : initial point; s : gradient sparsity level; α : step size; δ : query radius; J : number of blocks.
 $s_{\text{block}} \leftarrow 1.1s/J$
Randomly divide x into J equally sized blocks.
if ZO-BCD-R **then**
 $m \leftarrow b_1 s_{\text{block}} \log(d/J)$
Generate Rademacher random vectors z_1, \dots, z_m
else if ZO-BCD-RC **then**
 $m \leftarrow b_3 s_{\text{block}} \log^2(s_{\text{block}}) \log^2(d/J)$
Generate Rademacher random vector z .
Randomly choose $\Omega \subset \{1, \dots, d/J\}$ with $|\Omega| = m$
Let $z_i = \mathcal{C}_{j_i}(z)$ for $i = 1, \dots, m$ and $j_i \in \Omega$
end if
for $k = 0$ **to** K **do**
Select a block $j \in \{1, \dots, J\}$ uniformly at random.
 $\hat{g}_k^{(j)} \leftarrow \text{Gradient Estimation}(x_k^{(j)}, s_{\text{block}}, \delta, \{z_i\}_{i=1}^{m/J})$
 $x_{k+1} \leftarrow x_k - \alpha \hat{g}_k^{(j)}$
end for
Output: x_K : estimated optimum point.

Theorem 3.1. Assume that $f(x)$ satisfies Assumptions 1–6. Define the following constants:

$$\begin{aligned} L_{\max} &= \max_j L_j, \\ c_1 &= 2JL_{\max}\mathcal{R}^2(x_0), \\ H &= \max_j H_j. \end{aligned}$$

Assume that $4\rho^{4n} + \frac{16\tau^2\sigma H}{c_1 L_{\max}} < 1$. Choose sparsity $s \geq s_{\text{exact}}$, step size $\alpha = \frac{1}{L_{\max}}$ and query radius $\delta = 2\sqrt{\sigma/H}$. Choose the number of CoSaMP iterations n and error tolerance ε such that:

$$\frac{c_1}{2} \left(2\rho^{2n} + \sqrt{4\rho^{4n} + \frac{16\tau^2\sigma H}{c_1 \zeta L_{\max}}} \right) < \varepsilon < f(x_0) - f^*.$$

Then, with probability $1 - \zeta - \mathcal{O}\left(\frac{J^2}{\varepsilon} e^{-s_{\text{exact}}/J}\right)$ ZO-BCD finds an ε -optimal solution in $\tilde{\mathcal{O}}(s/\varepsilon)$ queries. ZO-BCD-R requires $\tilde{\mathcal{O}}(sd/J^2)$ FLOPS per iteration and $\tilde{\mathcal{O}}(sd/J^2)$ total memory, while ZO-BCD-RC requires only $\tilde{\mathcal{O}}(d/J)$ FLOPS per iteration and $\mathcal{O}(d/J)$ total memory.

Thus, up to logarithmic factors, ZO-BCD achieves the same query complexity as ZORO [11] with a much lower per-iteration computational footprint. Note that we pay for the

improved computational and memory complexity of ZO-BCD-RC with a slightly worse theoretical query complexity (by a logarithmic factor) due to the requirements of Theorem 2.4. First order block coordinate descent methods typically have a probability of success $1 - \zeta$, thus in switching to zeroth-order we incur a penalty of $\mathcal{O}\left(\frac{J^2}{\varepsilon} e^{-s_{\text{exact}}/J}\right)$. For truly huge problems (for example $d \approx 10^6$ and $s_{\text{exact}} \approx 10^4$) this term is negligible. For smaller problems we find that randomly re-assigning the decision variables to blocks every J iterations is a good way to increase ZO-BCD’s probability of success.

4 Sparse wavelet transform attacks

Adversarial attacks on neural-network-based classifiers are a popular application and benchmark for zeroth-order optimizers [8, 23–25]. Specifically, let $F(x) \in [0, 1]^C$ denote the predicted probabilities returned by the model for input signal x . Then the goal is to find a small distortion δ such that the model’s top-1 prediction on $x + \delta$ is no longer correct: $\text{argmax}_{c=1,\dots,C} F_c(x + \delta) \neq \text{argmax}_{c=1,\dots,C} F_c(x)$. Because we only have access to the logits, $F(x)$, not the internal workings of the model, we are unable to compute $\nabla F(x)$ and hence this problem is zeroth order. Recently, [11] showed that it is reasonable to assume that the attack loss function exhibits (approximate) gradient sparsity, and proposed generating adversarial examples by adding a distortion to the victim image that is sparse in the image pixel domain. We extend this and propose a novel *sparse wavelet transform attack*, which searches for an adversarial distortion δ^* in the wavelet domain:

$$\delta^* = \underset{\delta}{\operatorname{argmin}} f(\text{IWT}(\text{WT}(x) + \delta)) + \lambda \|\delta\|_0, \quad (7)$$

where x is a given image/audio signal, f is the Carlini-Wagner loss function [8], WT is the chosen (discrete or continuous) wavelet transform, and IWT is the corresponding inverse wavelet transform. As wavelet transforms extract the important features of the data, we expect the gradients of this new loss function to be even sparser than those of the corresponding pixel-domain loss function [11, Figure 1]. Moreover the inverse wavelet transform spreads the energy of the sparse perturbation, resulting in more natural-seeming attacked signals, as compared with pixel-domain sparse attacks [11, Figure 6].

1. **Sparse DWT attacks.** Discrete wavelet transform (DWT) is a well-known method for data compression and denoising [26, 27]. In fact, many real-world media data are compressed and stored in the form of DWT coefficients (*e.g.* JPEG-2000 for images and Dirac for videos), thus attacking the wavelet domain is more direct in these cases. Since DWT does not increase the problem dimension³, the query complexity of sparse wavelet-domain attacks is expected to be the same order as sparse pixel-domain

³Only with periodic boundary extension. If other boundary extension is used, the dimension of the wavelet coefficients will slightly increase, which depends on the size of wavelet filters and the level of wavelet transform.

attacks. An interesting variation is to only attack the important (*i.e.* large) wavelet coefficients. We explore this further in Section 5. This can reduce the attack problem dimension by 60%–80% for typical image datasets. Nevertheless, for large, modern color images, this problem dimension can still be massive.

2. **Sparse CWT attacks.** For oscillatory signals, the continuous wavelet transform (CWT) with analytic wavelets is preferred [26, 28]. Unlike DWT, the dimension of the CWT coefficients is much larger than the original signal dimension, which is the main challenge of the CWT attacks. For example, attacking even 1 second audio clips in a CWT domain results in a problem of size $d > 1.7$ million (see Section 5.3)!

Note that the idea of adversarial attacks on DWT coefficients was also proposed in [18], but they assume a white-box model and study only dense attacks on discrete Haar wavelets. [19] considers a “steganographic” attack, where the important wavelet coefficients of a target image are “hidden” within the wavelet transform coefficients of a victim image. We appear to be the first to connect (both discrete and continuous) wavelet transforms to sparse zeroth-order adversarial attacks.

5 Empirical results

In this section, we first present the empirical advantages of ZO-BCD with synthetic examples. Then, we demonstrate the performance of ZO-BCD in two real-world applications: (i) sparse DWT attacks on images, and (ii) sparse CWT attacks on audio signals. We compare the two versions of ZO-BCD (see Algorithm 2) against two venerable zeroth-order algorithms—FDSA [29] and SPSA⁴ [31]—as well as two more recent contributions—ZO-SCD [8] and ZORO [11]. ZO-SCD is a zeroth-order (non-block) coordinate descent method, while ZORO uses a similar gradient estimator as ZO-BCD, but uses it to compute the full gradient. We do not consider any methods that involve inverting a $d \times d$ matrix (such as CMA-ES [32]) as the goal here is to analyze the performance of zeroth-order algorithms for problems so large that this is not feasible. In Section 5.2, we consider ZO-SGD [33], a variance-reduced version of SPSA, as this has empirically shown better performance on this task than SPSA⁵. We also consider ZO-AdaMM [23], a zeroth-order method incorporating momentum. The numerical experiments in Section 5.1 were executed in Matlab 2020b on a laptop with Intel i7-8750H and 32GB of RAM.

5.1 Synthetic examples

We study the performance of ZO-BCD with noisy oracles on the zeroth-order optimization problem $\text{minimize}_{x \in \mathbb{R}^d} f(x)$ for two selected objective functions:

⁴We note that SPSA using Rademacher sample directions coincides with Random Search [30]

⁵Variance reduction did little to improve the performance of SPSA in the experiments of Section 5.1

(a) Sparse quadratic function: $f(x) = \frac{1}{2}x^T Ax$, where A is a diagonal matrix with s non-zero entries.

(b) Max- s -sum-squared function: $f(x) = \frac{1}{2} \sum_{m_i}^s x_{m_i}^2$, where x_{m_i} is the i -th largest-in-magnitude entry of x . Obviously, this problem is more complicated since m_i changes with different x .

We use $d = 20,000$ and $s = 200$ in both problems, so they have high ambient dimension with sparse gradients.

As can be seen in Figures 2a and 2b, both versions of ZO-BCD effectively exploit the gradient sparsity, and have very competitive performance in terms of queries. In particular, ZO-BCD converges more stably than the state-of-the-art ZORO in max- s -sum-squared-sum problem while its computational and memory complexities are much lower. Note that SPSA's query efficiency is roughly of the same order as that of ZO-BCD and ZORO when the gradient support is unchanging (Figure 2a); however, it is *significantly worse* when the gradient support is allowed to change (Figure 2b).

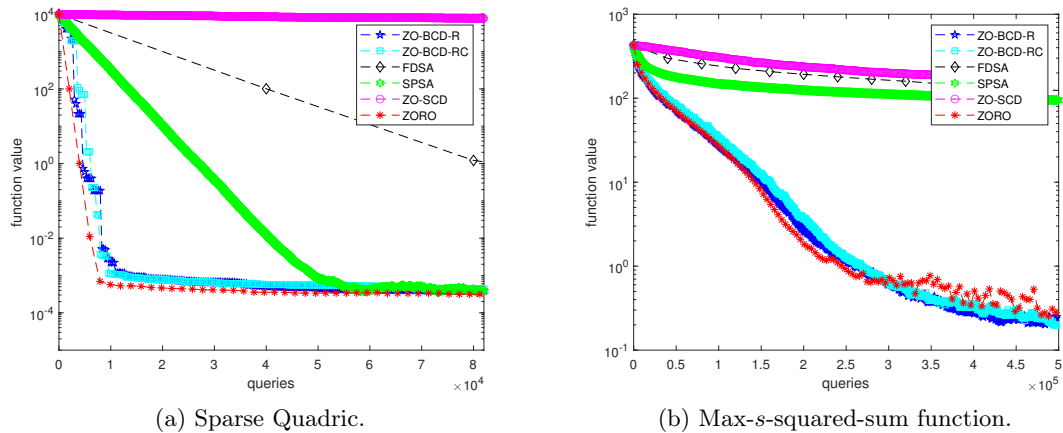


Figure 2: Function values *v.s.* queries for ZO-BCD (-R and -RC, with 5 blocks) and four other representative zeroth-order methods. ZO-BCD is fast and stable (while running faster with less memory).

Computational complexity. Since ZO-BCD and ZORO are the only methods that have competitive convergence rates in the query complexity experiments above, we only compare their computational complexities. We record the runtime of ZO-BCD and ZORO for solving the sparse quadratic function with stopping condition $f(x_k) \leq 10^{-2}$. Note that the runtime of each query can vary a lot between problems, so we only count the empirical runtime excluding the queries' time. The experimental results are presented in Figure 3, where one can see that ZO-BCD-R has significant speed advantage over ZORO

and ZO-BCD-RC is even faster.

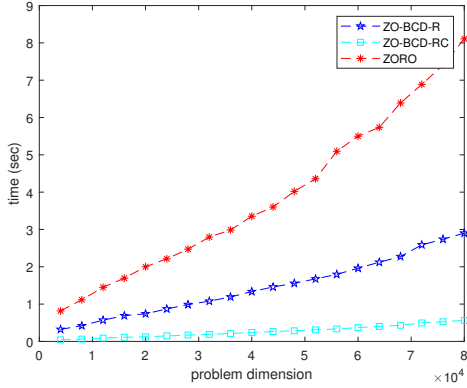


Figure 3: Runtime *v.s.* problem dimension for ZO-BCD (-R and -RC, with 5 blocks) and ZORO.

5.2 Sparse DWT attacks on images

We consider a wavelet domain, untargeted, per-image attack on the **ImageNet** dataset [34] with the pre-trained **Inception-v3** model [35], as discussed in Section 4. We use the famous ‘db45’ wavelet [36] with 3-level DWT in these attacks. Empirical performance was evaluated by attacking 1000 randomly selected **ImageNet** pictures that were initially classified correctly. In addition to full wavelet domain attacks using both ZO-BCD-R and ZO-BCD-RC, we also experiment with only attacking the large wavelet coefficients, *i.e.* the important components of the images in terms of wavelet basis. In particular, when we choose to only attack wavelet coefficients greater than 0.05 in magnitude, the problem dimension is reduced by an average 67.3% for the tested images; nevertheless, the attack problem dimension is still as large as $\sim 90,000$, so ZO-BCD is still suitable for this attack problem.

The results are summarized in Table 1. We find all three versions of ZO-BCD wavelet attack beat the other state-of-the-art methods in both attack success rate and ℓ_2 distortion, and the large-coefficients-only (*i.e.* we only attack wavelet coefficients with $\text{abs} \geq 0.05$) wavelet attack by ZO-BCD-R achieves the best results. We present a few visual examples of these adversarial attacks in Figure 4. More examples and the detailed experimental settings can be found in Appendix D.

5.3 Sparse CWT attacks on audio signals

We consider targeted per-clip audio adversarial attacks on the **SpeechCommands** dataset [37], which consists of 1-second audio clips, each containing a one-word voice command, *e.g.* “yes” or “left”. The audio sampling rate is 16kHz, thus, each clip is a 16,000 dimension real valued

Table 1: Results of untargeted image adversarial attack from various algorithms. Attack success rate (ASR), average final ℓ_0 distortion (as a percentage of total pixel numbers), average final ℓ_2 distortion (on pixel domain), average final ℓ_2 distortion on frequency (wavelet) domain, average iterations and number of queries of 1st successful attack for different zeroth-order attack methods. ZO-BCD-R(large coeff.) stands for applying ZO-BCD-R to attack only large wavelet coefficients ($\text{abs} \geq 0.05$).

METHODS	ASR	ℓ_2 DIST	QUERIES
ZO-SCD	78%	57.5	2400
ZO-SGD	78%	37.9	1590
ZO-AdaMM	81%	28.2	1720
ZORO	90%	21.1	2950
ZO-BCD-R	92%	14.1	2131
ZO-BCD-RC	92%	14.2	2090
ZO-BCD-R(large coeff.)	96%	13.7	1662

vector. Adversarial attacks against this data set have been considered in [10, 38, 39] and [40], although with the exception of [10] all of the cited works consider a white-box setting⁶. The victim model is a pre-trained, 5 layer, convolutional network called `commandNet` [41]. The architecture is essentially as proposed in [42]. It takes as input the bark spectrum coefficients of a given audio clip, a transform that is closely related to the Mel Frequency transform. The test classification accuracy of this model (on un-attacked audio clips) is 94.46%. We use the Morse [43] continuous wavelet transform with 111 frequencies, resulting in a problem dimension of $111 \times 16,000 = 1,776,000$. As discussed in [44], the appropriate measure of size for the attacking distortion δ is relative loudness:

$$\text{dB}_x(\delta) := 20 \left(\max_i \log_{10}(|x_i|) - \max_i \log_{10}(|\delta_i|) \right).$$

The results of our attack are detailed in Table 2, Figures 5a and 5b. Overall, we achieve a 97.93% ASR using a mean of 7073 queries. Our attacking distortions have a mean volume of -6.32dB . As can be seen, our proposed attack comfortably exceeds the state of the art in attack success rate (ASR), surpassing even white-box attacks! This is not to claim that our proposed method is strictly better than others, as there are multiple factors to consider when judging the “goodness” of an attack (ASR, attack distortion, universality etc). We discuss this further in Appendix E.2. The attacking noise can be heard as a slight “hiss”, or white noise in the attacked audio clips. The original keyword however is easy for a human

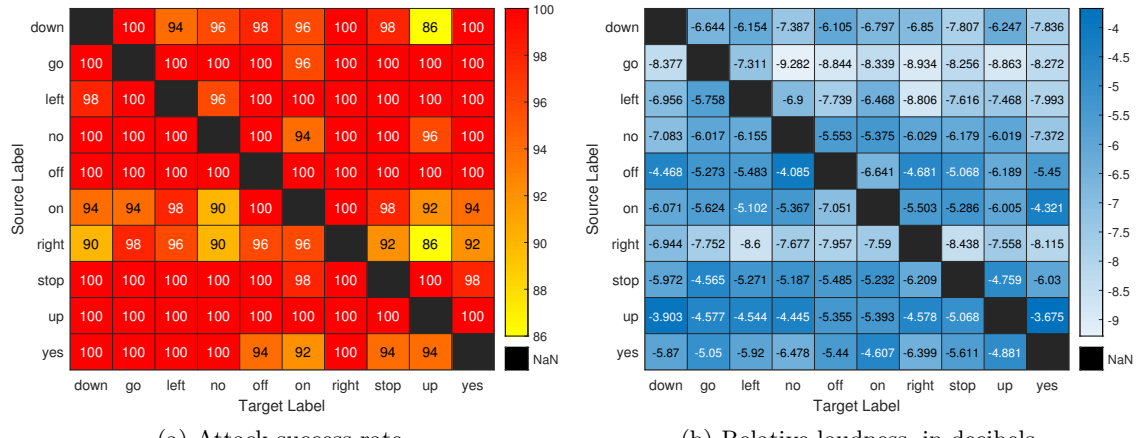
⁶There are other subtle differences in the threat models considered in these works, as compared to ours. We discuss this further in Appendix E.2



(a) ZO-BCD-R: “barber- (b) ZO-BCD-R (large co- (c) ZO-BCD-R: “dumbbell” (d) ZO-BCD-R (large co-
shop” → “flagpole” eff.): “barbershop” → “flag- → “computer keyboard” eff.): “dumbbell” → “com-
pole” pole” puter keyboard”

Figure 4: Examples of wavelet attacked images by ZO-BCD-R and ZO-BCD-R (attack restricted to only large coefficients, *i.e.* $\text{abs} \geq 0.05$), true labels and mis-classified labels.

listener to make out. We encourage the reader to listen to a few examples, available at <https://github.com/YuchenLou/ZO-BCD>.



(a) Attack success rate.

(b) Relative loudness, in decibels

Figure 5: Detailed results for *targeted* audio wavelet attacks.

Out of curiosity, we also tested untargeted crafting adversarial attacks using ZO-BCD in the time domain (*i.e.* without using a wavelet transform) for 1000 randomly selected audio clips. The results are underwhelming; indeed the attacking perturbation is on average significantly *louder* than the victim audio clip (see Table 3)! This suggests that attacking in a wavelet domain is much more effective than attacking in the original signal domain.

Table 2: Results of adversarial attacks on the `SpeechCommand` data set

METHODS	ASR	UNIV.	BLACK-BOX	TARGETED
Alzentot [10]	89.0%	No	YES	YES
Vadillo & Santana [38]	70.4%	YES	No	No
Li <i>et al</i> [39]	96.8%	YES	No	YES
Xie <i>et al</i> [40]	97.8%	No	No	YES
Proposed	97.9%	No	YES	YES

Table 3: Results for *untargeted* audio wavelet attack. Attack success rate (ASR), average final Decibel distortion, average number of queries to 1st successful attack for *untargeted* zeroth-order attack in the time domain, in the wavelet domain using a step-size of 0.02 and in the wavelet domain using a step-size of 0.05.

DOMAINS	ASR	dB DIST	QUERIES
Time	100%	+1.5597	894
Wavelet (0.02)	99.9%	-13.8939	3452
Wavelet (0.05)	100%	-7.1192	2502

6 Conclusion

We have introduced ZO-BCD, a novel zeroth-order optimization algorithm. ZO-BCD enjoys strong, albeit probabilistic, convergence guarantees. We have also introduced a new paradigm in adversarial attacks on classifiers: the sparse wavelet domain attack. On medium-scale test problems the performance of ZO-BCD matches or exceeds that of state-of-the-art zeroth order optimization algorithms, as predicted by theory. However, the low per-iteration computational and memory requirements of ZO-BCD means that it can tackle huge-scale problems that for other zeroth-order algorithms are intractable. We demonstrate this by successfully using ZO-BCD to craft adversarial examples, to both image and audio classifiers, in wavelet domains where the problem size can exceed 1.7 million.

References

[1] B Reeja-Jayan, Katharine L Harrison, K Yang, Chih-Liang Wang, AE Yilmaz, and Arumugam Manthiram. Microwave-assisted low-temperature growth of thin films in solution. *Scientific reports*, 2(1):1–8, 2012.

- [2] Frank Hutter, Holger Hoos, and Kevin Leyton-Brown. An efficient approach for assessing hyperparameter importance. In *International conference on machine learning*, pages 754–762. PMLR, 2014.
- [3] James Bergstra and Yoshua Bengio. Random search for hyper-parameter optimization. *Journal of machine learning research*, 13(2), 2012.
- [4] Abraham D Flaxman, Adam Tauman Kalai, and H Brendan McMahan. Online convex optimization in the bandit setting: gradient descent without a gradient. In *Proceedings of the sixteenth annual ACM-SIAM symposium on Discrete algorithms*, pages 385–394, 2005.
- [5] Tim Salimans, Jonathan Ho, Xi Chen, Szymon Sidor, and Ilya Sutskever. Evolution strategies as a scalable alternative to reinforcement learning. *arXiv preprint arXiv:1703.03864*, 2017.
- [6] Horia Mania, Aurelia Guy, and Benjamin Recht. Simple random search of static linear policies is competitive for reinforcement learning. In *Proceedings of the 32nd International Conference on Neural Information Processing Systems*, pages 1805–1814, 2018.
- [7] Krzysztof Choromanski, Aldo Pacchiano, Jack Parker-Holder, Yunhao Tang, Deepali Jain, Yuxiang Yang, Atil Iscen, Jasmine Hsu, and Vikas Sindhwani. Provably robust blackbox optimization for reinforcement learning. In *Conference on Robot Learning*, pages 683–696. PMLR, 2020.
- [8] Pin-Yu Chen, Huan Zhang, Yash Sharma, Jinfeng Yi, and Cho-Jui Hsieh. Zoo: Zeroth order optimization based black-box attacks to deep neural networks without training substitute models. In *Proceedings of the 10th ACM workshop on artificial intelligence and security*, pages 15–26, 2017.
- [9] Xiangru Lian, Huan Zhang, Cho-Jui Hsieh, Yijun Huang, and Ji Liu. A comprehensive linear speedup analysis for asynchronous stochastic parallel optimization from zeroth-order to first-order. *arXiv preprint arXiv:1606.00498*, 2016.
- [10] Moustafa Alzantot, Bharathan Balaji, and Mani Srivastava. Did you hear that? adversarial examples against automatic speech recognition. *arXiv preprint arXiv:1801.00554*, 2018.
- [11] HanQin Cai, Daniel Mckenzie, Wotao Yin, and Zhenliang Zhang. Zeroth-order regularized optimization (ZORO): Approximately sparse gradients and adaptive sampling. *arXiv preprint arXiv:2003.13001*, 2020.
- [12] Kevin G Jamieson, Robert D Nowak, and Benjamin Recht. Query complexity of derivative-free optimization. *arXiv preprint arXiv:1209.2434*, 2012.

- [13] Yining Wang, Simon Du, Sivaraman Balakrishnan, and Aarti Singh. Stochastic zeroth-order optimization in high dimensions. In *International Conference on Artificial Intelligence and Statistics*, pages 1356–1365, 2018.
- [14] Krishnakumar Balasubramanian and Saeed Ghadimi. Zeroth-order (non)-convex stochastic optimization via conditional gradient and gradient updates. In *Advances in Neural Information Processing Systems*, pages 3455–3464, 2018.
- [15] Daniel Golovin, John Karro, Greg Kochanski, Chansoo Lee, Xingyou Song, and Qiuyi Zhang. Gradientless descent: High-dimensional zeroth-order optimization. In *International Conference on Learning Representations*, 2019.
- [16] Moustafa Alzantot, Yash Sharma, Supriyo Chakraborty, Huan Zhang, Cho-Jui Hsieh, and Mani B Srivastava. Genattack: Practical black-box attacks with gradient-free optimization. In *Proceedings of the Genetic and Evolutionary Computation Conference*, pages 1111–1119, 2019.
- [17] Rohan Taori, Amog Kamsetty, Brenton Chu, and Nikita Vemuri. Targeted adversarial examples for black box audio systems. In *2019 IEEE Security and Privacy Workshops (SPW)*, pages 15–20. IEEE, 2019.
- [18] Divyam Anshumaan, Akshay Agarwal, Mayank Vatsa, and Richa Singh. Wavetransform: Crafting adversarial examples via input decomposition. In *Computer Vision – ECCV 2020 Workshops*, pages 152–168. Springer, Cham, 2020.
- [19] Salah Ud Din, Naveed Akhtar, Shahzad Younis, Faisal Shafait, Atif Mansoor, and Muhammad Shafique. Steganographic universal adversarial perturbations. *Pattern Recognition Letters*, 135:146–152, 2020.
- [20] Rachael Tappenden, Peter Richtárik, and Jacek Gondzio. Inexact coordinate descent: complexity and preconditioning. *Journal of Optimization Theory and Applications*, 170(1):144–176, 2016.
- [21] Yu Nesterov. Efficiency of coordinate descent methods on huge-scale optimization problems. *SIAM Journal on Optimization*, 22(2):341–362, 2012.
- [22] Deanna Needell and Joel A Tropp. Cosamp: Iterative signal recovery from incomplete and inaccurate samples. *Applied and computational harmonic analysis*, 26(3):301–321, 2009.
- [23] Xiangyi Chen, Sijia Liu, Kaidi Xu, Xingguo Li, Xue Lin, Mingyi Hong, and David Cox. Zo-adamm: Zeroth-order adaptive momentum method for black-box optimization. In *Advances in Neural Information Processing Systems*, pages 7204–7215, 2019.

- [24] Andrew Ilyas, Logan Engstrom, Anish Athalye, and Jessy Lin. Black-box adversarial attacks with limited queries and information. In *International Conference on Machine Learning*, pages 2137–2146. PMLR, 2018.
- [25] Apostolos Modas, Seyed-Mohsen Moosavi-Dezfooli, and Pascal Frossard. Sparsefool: a few pixels make a big difference. In *Proceedings of the IEEE Conference on Computer Vision and Pattern Recognition*, pages 9087–9096, 2019.
- [26] Stéphane Mallat. *A wavelet tour of signal processing*. Elsevier, 1999.
- [27] Jian-Feng Cai, Bin Dong, Stanley Osher, and Zuowei Shen. Image restoration: total variation, wavelet frames, and beyond. *Journal of the American Mathematical Society*, 25(4):1033–1089, 2012.
- [28] Jonathan M Lilly and Sofia C Olhede. On the analytic wavelet transform. *IEEE transactions on information theory*, 56(8):4135–4156, 2010.
- [29] Jack Kiefer, Jacob Wolfowitz, et al. Stochastic estimation of the maximum of a regression function. *The Annals of Mathematical Statistics*, 23(3):462–466, 1952.
- [30] Yurii Nesterov and Vladimir Spokoiny. Random gradient-free minimization of convex functions. *Foundations of Computational Mathematics*, 17(2):527–566, 2017.
- [31] James C Spall. An overview of the simultaneous perturbation method for efficient optimization. *Johns Hopkins apl technical digest*, 19(4):482–492, 1998.
- [32] Nikolaus Hansen and Andreas Ostermeier. Completely derandomized self-adaptation in evolution strategies. *Evolutionary computation*, 9(2):159–195, 2001.
- [33] Saeed Ghadimi and Guanghui Lan. Stochastic first-and zeroth-order methods for nonconvex stochastic programming. *SIAM Journal on Optimization*, 23(4):2341–2368, 2013.
- [34] Jia Deng, Wei Dong, Richard Socher, Li-Jia Li, Kai Li, and Li Fei-Fei. Imagenet: A large-scale hierarchical image database. In *2009 IEEE conference on computer vision and pattern recognition*, pages 248–255. Ieee, 2009.
- [35] Christian Szegedy, Vincent Vanhoucke, Sergey Ioffe, Jon Shlens, and Zbigniew Wojna. Rethinking the inception architecture for computer vision. In *Proceedings of the IEEE conference on computer vision and pattern recognition*, pages 2818–2826, 2016.
- [36] Ingrid Daubechies. *Ten lectures on wavelets*. SIAM, 1992.
- [37] Pete Warden. Speech commands: A dataset for limited-vocabulary speech recognition. *arXiv preprint arXiv:1804.03209*, 2018.

- [38] Jon Vadillo and Roberto Santana. Universal adversarial examples in speech command classification. *arXiv preprint arXiv:1911.10182*, 2019.
- [39] Zhuohang Li, Yi Wu, Jian Liu, Yingying Chen, and Bo Yuan. Advpulse: Universal, synchronization-free, and targeted audio adversarial attacks via subsecond perturbations. In *Proceedings of the 2020 ACM SIGSAC Conference on Computer and Communications Security*, pages 1121–1134, 2020.
- [40] Yi Xie, Zhuohang Li, Cong Shi, Jian Liu, Yingying Chen, and Bo Yuan. Enabling fast and universal audio adversarial attack using generative model. *arXiv preprint arXiv:2004.12261*, 2020.
- [41] The MathWorks Inc. Speech command recognition using deep learning. <https://www.mathworks.com/help/deeplearning/ug/deep-learning-speech-recognition.html>, 2020. Accessed: 2021-01-15.
- [42] Tara N Sainath and Carolina Parada. Convolutional neural networks for small-footprint keyword spotting. In *Sixteenth Annual Conference of the International Speech Communication Association*, 2015.
- [43] Sofia C Olhede and Andrew T Walden. Generalized morse wavelets. *IEEE Transactions on Signal Processing*, 50(11):2661–2670, 2002.
- [44] Nicholas Carlini and David Wagner. Audio adversarial examples: Targeted attacks on speech-to-text. In *2018 IEEE Security and Privacy Workshops (SPW)*, pages 1–7. IEEE, 2018.
- [45] Felix Krahmer, Shahar Mendelson, and Holger Rauhut. Suprema of chaos processes and the restricted isometry property. *Communications on Pure and Applied Mathematics*, 67(11):1877–1904, 2014.
- [46] Shahar Mendelson, Holger Rauhut, Rachel Ward, et al. Improved bounds for sparse recovery from subsampled random convolutions. *The Annals of Applied Probability*, 28(6):3491–3527, 2018.
- [47] Meng Huang, Yuxuan Pang, and Zhiqiang Xu. Improved bounds for the rip of subsampled circulant matrices. *arXiv preprint arXiv:1808.07333*, 2018.
- [48] Dimitri P Bertsekas. Nonlinear programming. *Journal of the Operational Research Society*, 48(3):334–334, 1997.
- [49] Moustapha Cisse, Yossi Adi, Natalia Neverova, and Joseph Keshet. Houdini: Fooling deep structured visual and speech recognition models with adversarial examples. In *Proceedings of the 31st International Conference on Neural Information Processing Systems*, pages 6980–6990, 2017.

[50] Awni Hannun, Carl Case, Jared Casper, Bryan Catanzaro, Greg Diamos, Erich Elsen, Ryan Prenger, Sanjeev Satheesh, Shubho Sengupta, Adam Coates, et al. Deep speech: Scaling up end-to-end speech recognition. *arXiv preprint arXiv:1412.5567*, 2014.

A Proofs for Section 2

Proof of Theorem 2.1. Consider the function $f^{(j)}(t) = f(x + U^{(j)}t)$. This function has gradient $g^{(j)}$ and Hessian $\nabla_{jj}^2 f$. By Assumption 5 we have that $\|g^{(j)}\|_0 \leq \|g\|_0 \leq s$ while from Assumption 6 we have that $\|\nabla_{jj}^2 f\|_1 \leq H_j$. Thus, $f^{(j)}(t)$ satisfies all the assumptions of Theorem 2.6 and Corollary 2.7 of [11] and hence Theorem 2.1 follows from the conclusions of these two results. \square

Proof of Theorem 2.2. For notational convenience, we will temporarily let $s := s_{\text{exact}}$. Let g_{i_1}, \dots, g_{i_s} denote the non-zero entries of g , after the permutation has been applied. Let Y_j be a random variable counting the number of g_{i_k} within block j . That is:

$$Y_j = \#\{i_k : i_k \text{ in block } j\}.$$

Thus, the random vector $\mathbf{Y} = (Y_1, \dots, Y_J) \in \mathbb{R}^J$ satisfies the multinomial distribution. Observe that $\sum_{j=1}^J Y_j = s$ and, because the blocks are equally sized, $\mathbb{E}(Y_j) = \frac{s}{J}$.

By Chernoff's bound, for $\Delta > 0$ and each Y_j individually we have:

$$\mathbb{P} \left[\left| Y_j - \frac{s}{J} \right| \geq \Delta \frac{s}{J} \right] \leq 2e^{-\frac{\Delta^2 \mathbb{E}(Y_j)}{3}} = 2e^{-\frac{\Delta^2 s}{3J}}.$$

Then by applying the union bound to Y_j , we have:

$$\mathbb{P} \left[\exists j \text{ s.t. } \left| Y_j - \frac{s}{J} \right| \geq \Delta \frac{s}{J} \right] \leq \sum_{j=1}^J \mathbb{P} \left[\left| Y_j - \frac{s}{J} \right| \geq \Delta \frac{s}{J} \right] \leq 2J e^{-\frac{\Delta^2 s}{3J}},$$

and so:

$$\begin{aligned} \mathbb{P} \left[\left| Y_j - \frac{s}{J} \right| \leq \Delta \frac{s}{J}, \forall j \in [1, \dots, J] \right] &= 1 - \mathbb{P} \left[\exists j \text{ s.t. } \left| Y_j - \frac{s}{J} \right| \geq \Delta \frac{s}{J} \right] \\ &\geq 1 - 2J e^{-\frac{\Delta^2 s}{3J}}. \end{aligned}$$

This finishes the proof. \square

Proof of Corollary 2.3. From Theorem 2.2 we have that, with probability at least $1 - 2J \exp(-\frac{1.1^2 s_{\text{exact}}}{3J})$, $\|g^{(j)}\|_0 \leq 1.1 s_{\text{exact}} / J$. Assuming this is true, (5) holds with probability

$1 - (s/d)^{b_2 s}$, by tracing the arguments of Theorem 2.6 and Corollary 2.7 of [11] again. These events are independent, thus the probability that they both occur is:

$$\left(1 - 2J \exp\left(\frac{-1.1^2 s_{\text{exact}}}{3J}\right)\right) \left(1 - (s/d)^{b_2 s}\right)$$

Because $s_{\text{exact}} \ll d$ the term proportional to $\exp(-s_{\text{exact}}/J)$ is significantly larger than $(s/d)^{b_2 s}$. Expanding, and keeping only dominant terms we see that this probability is equal to $1 - \mathcal{O}(J \exp(-s_{\text{exact}}/J))$. \square

We emphasize that Corollary 2.3 holds for all j . Before proceeding, we remind the reader that for fixed s the *restricted isometry constant* of $Z \in \mathbb{R}^{m \times n}$ is defined as the smallest $\delta > 0$ such that:

$$(1 - \delta) \|v\|_2^2 \leq \|Zv\|_2^2 \leq (1 + \delta) \|v\|_2^2 \quad \text{for all } v \in \mathbb{R}^n \text{ satisfying } \|v\|_0 \leq s$$

The key ingredient to the proof of Theorem 2.4 is the following result:

Theorem A.1 ([45, Theorem 1.1]). *Let $z \in \mathbb{R}^n$ be a Rademacher random vector and choose a random subset $\Omega = \{j_1, \dots, j_m\} \subset \{1, \dots, d/J\}$ of cardinality $m = c\delta^{-2}s \log^2(s) \log^2(n)$. Let $Z \in \mathbb{R}^{m \times n}$ denote the matrix with rows $\frac{1}{\sqrt{m}}\mathcal{C}_{j_i}(z)$. Then $\delta_s(Z) < \delta$ with probability $1 - n^{-\log(n) \log^2(s)}$.*

Note that c is a universal constant, independent of s, n and δ . Similar results may be found in [46] and [47]. In [45] a more general version of this theorem is provided, which allows the entries of z to be drawn from any sub-Gaussian distribution.

Proof of Theorem 2.4. As before, from Theorem 2.2 we have that $\|g^{(j)}\|_0 \leq 1.1s_{\text{exact}}/J$ with probability at least $1 - 2J \exp\left(\frac{-1.1^2 s_{\text{exact}}}{3J}\right)$. Assuming this holds, let Z be the sensing matrix with rows $\frac{1}{\sqrt{m}}\mathcal{C}_{j_i}(z)$. By appealing to Theorem A.1 with $s = 4.4s_{\text{exact}}/J$, $n = d/J$ and $\delta = 0.3843$ we get that $\delta_{4s}(Z) \leq 0.3843$, with probability $1 - (d/J)^{-\log(d/J) \log^2(s)}$. Once this restricted isometry property has been guaranteed, Theorem 2.4 follows by the same proof as in [11, Corollary 2.7]. As argued in the proof of Corollary 2.3 the events $\|g^{(j)}\|_0 \leq 1.1s_{\text{exact}}/J$ and $\delta_{4s}(Z) \leq 0.3843$ are independent, hence they both occur with probability:

$$\left(1 - 2J \exp\left(\frac{-1.1^2 s_{\text{exact}}}{3J}\right)\right) \left(1 - (d/J)^{-\log(d/J) \log^2(s)}\right)$$

Again, the term proportional to $\exp(-s_{\text{exact}}/J)$ dominates. \square

B ZO-BCD for unequally-sized blocks

Using randomly assigned, equally-sized blocks is an important part of the ZO-BCD framework as it allows one to consider a block sparsity $\approx s/J$, instead of the worst case sparsity of s . Nevertheless, there may be situations where it is preferable to use user-defined, unequally-sized blocks. For such cases we recommend the following (we discuss the modifications here for ZO-BCD-R, but with obvious changes it also applies to ZO-BCD-RC). Let $s^{(j)} \leq s$ be an upper estimate of the sparsity of the j -th block gradient: $\|g^{(j)}(x)\|_0 \leq s^{(j)}$. Let $m^{(j)} = b_1 s^{(j)} \log(d/J)$ (and use the analogous formula for ZO-BCD-RC) and define $m^{\max} = \max_j m^{(j)}$. When initializing ZO-BCD-R, generate m^{\max} Rademacher random variables: $z_1, \dots, z_{m^{\max}} \in \mathbb{R}^{d^{\max}}$. At each iteration, if block j is selected, randomly select $i_1, \dots, i_{m^{(j)}}$ from $1, \dots, m^{\max}$ and for $k = 1, \dots, m^{(j)}$ let $\tilde{z}_{i_k} \in \mathbb{R}^{d^{(j)}}$ denote the vector formed by taking the first $d^{(j)}$ components of z_{i_k} . Use $\{\tilde{z}_{i_k}\}_{k=1}^{m^{(j)}}$ as the input to Algorithm 1. Note that the $\{\tilde{z}_{i_k}\}_{k=1}^{m^{(j)}}$ possess the same statistical properties as the $\{z_{i_k}\}_{k=1}^{m^{(j)}}$ (*i.e.* they are i.i.d. Rademacher vectors) so using them as sampling directions will result in the same bound on $\|g_k^{(j)} - \hat{g}_k^{(j)}\|$ as Corollary 2.3.

C Proofs for Section 3

Our proof utilizes the main result of [20]. Note that this paper requires that $\alpha_k = \frac{1}{L_{j_k}}$, *i.e.* the step size at the k -th iteration is inversely proportional to the block Lipschitz constant. This is certainly ideal, but impractical. In particular, if the blocks are randomly selected it seems implausible that one would have good estimates of the L_j . Of course, since $L_j \leq L_{\max}$ we observe that L_{\max} is a Lipschitz constant for every block, and thus we may indeed take $\alpha_k = \alpha = \frac{1}{L_{\max}}$. This results in a slightly slower convergence resulted, reflected in a factor of L_{\max} in Theorem 3.1. Throughout this section we shall assume that $f(x)$ satisfies Assumptions 1–6. For all $j = 1, \dots, J$ define:

$$V_j(x, t) = \langle g^{(j)}(x), t \rangle + \frac{L_{\max}}{2} \|t\|_2^2,$$

so that, by Lipschitz differentiability:

$$f(x_k + U^{(j)}t) \leq f(x_k) + V_j(x_k, t).$$

Define $t_{k,j}^* := \operatorname{argmin} V_j(x_k, t) := -\frac{1}{L_{\max}} g_k^{(j)}$ while let $t'_{k,j}$ be the update step taken by ZO-BCD, *i.e.* $t'_{k,j} = \frac{1}{L_{\max}} \hat{g}_k^{(j)}$.

Lemma C.1. *Suppose that f satisfies Assumptions 1–3. Then $f(x) - f^* \geq \frac{1}{2L_{\max}} \|g^{(j)}(x)\|_2^2$ for any $x \in \mathbb{R}^d$ and any $j = 1, \dots, J$.*

Proof. Define $h_x : \mathbb{R}^{d^{(j)}} \rightarrow \mathbb{R}$ as $h_x(t) := f(x + U^{(j)}t)$ where $U^{(j)}$ is as described in Section 1. Since $U^{(j)}$ is a linear transformation and $f(x)$ is convex, h_x is also convex. By Assumption 1 and the fact that $L_j \leq L_{\max}$, h_x is L_{\max} -Lipschitz differentiable. From Assumption 3 it follows that $\mathcal{Y}^* = \operatorname{argmin}_t h_x(t)$ is non-empty, and that $h_x^* := \min_t h_x(t) \geq f^*$. Thus, from [48, Proposition B.3, part (c.ii)], we have:

$$h_x(t) - h_x^* \geq \frac{1}{2L_{\max}} \|\nabla h_x(t)\|_2^2 = \frac{1}{2L_{\max}} \|g^{(j)}(x + U^{(j)}t)\|_2^2$$

for all t . Choose $t = 0$, and use the facts that $h_x(0) = f(x)$ and $f^* \leq h_x^*$ to obtain:

$$f(x) - f^* \geq h_x(0) - h_x^* \geq \frac{1}{2L_{\max}} \|g^{(j)}(x)\|_2^2.$$

This finishes the proof. \square

Lemma C.2. *Let $\eta = 2\rho^{2n}$ and $\theta = \frac{4\tau^2\sigma H}{L_{\max}}$. Then for each iteration of ZO-BCD we have that:*

$$V_j(x_k, t') - V_j(x_k, t^*) \leq \eta(f(x_k) - f^*) + \theta. \quad (8)$$

with probability $1 - \mathcal{O}(J \exp(-s_{\text{exact}}/J))$.

Proof. For notational convenience, we define $t^* := t_{k,j}^*$, $t' := t'_{k,j}$ and $e_k^{(j)} := \hat{g}_k^{(j)} - g_k^{(j)}$. By definition:

$$t'_{k,j} = -\frac{1}{L_{\max}} \hat{g}_k^{(j)} = -\frac{1}{L_{\max}} (g_k^{(j)} + e_k^{(j)}).$$

Moreover:

$$\begin{aligned} V_j(x_k, t^*) &= -\frac{1}{2L_{\max}} \|g_k^{(j)}\|_2^2 \\ V_j(x_k, t') &= -\frac{1}{2L_{\max}} \|g_k^{(j)}\|_2^2 + \frac{1}{2L_{\max}} \|e_k^{(j)}\|_2^2, \end{aligned}$$

and hence:

$$V_j(x_k, t') - V_j(x_k, t^*) \leq \frac{1}{2L_{\max}} \|e_k^{(j)}\|_2^2. \quad (9)$$

Because $H_j \leq H$ for all j , from Corollary 2.3 (for ZO-BCD-R) or Theorem 2.4 (for ZO-BCD-RC) we have that:

$$\begin{aligned} \|e_k^{(j)}\|_2^2 &\leq \left(\rho^n \|g_k^{(j)}\|_2 + 2\tau\sqrt{\sigma H} \right)^2 \\ &\leq 2\rho^{2n} \|g_k^{(j)}\|_2^2 + 4\tau^2\sigma H. \end{aligned} \quad (10)$$

with probability $1 - \mathcal{O}(J \exp(-s_{\text{exact}}/J))$. Finally, from Lemma C.1 we get that $\|g_k^{(j)}\|_2^2 \leq 2L_{\max}(f(x_k) - f^*)$ for any $j = 1, \dots, J$. Connecting this estimate with (9) and (10) we obtain:

$$V_j(x_k, t') - V_j(x_k, t^*) \leq \underbrace{2\rho^{2n}}_{=\eta} (f(x_k) - f^*) + \underbrace{\frac{4\tau^2\sigma H}{L_{\max}}}_{=\theta}.$$

This finishes the proof. \square

Proof of Theorem 3.1. Let p_j denote the probability that the j -th block is chosen for updating at the k -th iteration. Because ZO-BCD chooses blocks uniformly at random, $p_j = 1/J$ for all j . If (8) holds for all k then by [20, Theorem 6.1] if:

$$\begin{aligned} \eta^2 + \frac{4\theta}{c_1} &< 1 \text{ where } c_1 = 2JL_{\max}\mathcal{R}^2(x_0), \\ \frac{c_1}{2}(\eta + \sqrt{\eta^2 + \frac{4\theta}{c_1\zeta}}) &< \varepsilon < f(x_0) - f^*, \\ u &:= \frac{c_1}{2} \left(\eta + \sqrt{\eta^2 + \frac{4\theta}{c_1}} \right), \\ K &:= \frac{c_1}{\varepsilon - u} + \frac{c_1}{\varepsilon - \eta c_1} \log \left(\frac{\varepsilon - \frac{\theta c_1}{\varepsilon - \eta c_1}}{\varepsilon \zeta - \frac{\theta c_1}{\varepsilon - \eta c_1}} \right) + 2, \end{aligned}$$

then $\mathbb{P}(f(x_K) - f^* \leq \varepsilon) \geq 1 - \zeta$. Note that:

- Our η and θ are α and β in their notation.
- In [20] $c_1 = 2\mathcal{R}_{\ell_{p-1}}^2(x_0)$ where $\mathcal{R}_{\ell_{p-1}}^2(x_0)$ is defined as in (2) but using a norm $\|\cdot\|_{\ell_{p-1}}$ instead of $\|\cdot\|_2$. These norms are related as:

$$\|x\|_{\ell_{p-1}}^2 = \sum_{j=1}^J \frac{L_j}{p_j} \|x^{(j)}\|_2^2 \stackrel{(a)}{=} \sum_{j=1}^J JL_{\max} \|x^{(j)}\|_2^2 = JL_{\max} \|x\|_2^2$$

where (a) follows as $p_j = 1/J$ for all j and we are taking $L_j = L_{\max}$. Hence, $c_1 = 2JL_{\max}\mathcal{R}^2(x_0)$ as stated.

Replace η and θ with the expressions given by Lemma C.2 to obtain the expressions given in the statement of Theorem 3.1. Because (8) holds with probability $1 - \mathcal{O}(J \exp(-s_{\text{exact}}/J))$ at each iteration, by the union bound it holds with probability:

$$1 - K\mathcal{O}(J \exp(-s_{\text{exact}}/J)) = 1 - \mathcal{O}\left(\frac{J^2}{\varepsilon} \exp\left(-\frac{s_{\text{exact}}}{J}\right)\right)$$

for all K iterations. Applying the union bound again we obtain:

$$\begin{aligned}\mathbb{P}(f(x_K) - f^* \leq \varepsilon) &\geq (1 - \zeta) \left(1 - \mathcal{O} \left(\frac{J^2}{\varepsilon} \exp \left(-\frac{s_{\text{exact}}}{J} \right) \right) \right) \\ &= 1 - \zeta - \mathcal{O} \left(\frac{J^2}{\varepsilon} \exp \left(-\frac{s_{\text{exact}}}{J} \right) \right).\end{aligned}$$

ZO-BCD-R makes $m = 1.1b_1(s/J) \log(d/J)$ queries per iteration, and hence makes:

$$\begin{aligned}mK &= 1.1b_1 \frac{s}{J} \log \left(\frac{d}{J} \right) K \\ &= \frac{1.1b_1 s \log(d/J) \mathcal{R}^2(x_0)}{\varepsilon - u} + \frac{1.1b_1 s \log(d/J) \mathcal{R}^2(x_0)}{\varepsilon - 2\eta J \mathcal{R}^2(x_0)} \log \left(\frac{\varepsilon - \frac{\theta c_1}{\varepsilon - \eta c_1}}{\varepsilon \zeta - \frac{\theta c_1}{\varepsilon - \eta c_1}} \right) + 2.2b_1 \frac{s}{J} \log \left(\frac{d}{J} \right) \\ &= \mathcal{O} \left(\frac{s \log(d/J)}{\varepsilon} \right) = \tilde{\mathcal{O}} \left(\frac{s}{\varepsilon} \right)\end{aligned}$$

queries in total. On the other hand, ZO-BCD-RC makes $m = 1.1b_3(s/J) \log^2(s/J) \log^2(d/J)$ queries per iteration. A similar calculation reveals that:

$$mK = \mathcal{O} \left(\frac{s \log^2(s/J) \log^2(d/J)}{\varepsilon} \right) = \tilde{\mathcal{O}} \left(\frac{s}{\varepsilon} \right).$$

The computational cost of each iteration is dominated by solving the sparse recovery problem using CoSaMP. It is known [22] that CoSaMP requires $\mathcal{O}(n\mathcal{T})$ FLOPS, where \mathcal{T} is the cost of a matrix-vector multiply by Z . For ZO-BCD-R $Z \in \mathbb{R}^{m \times (d/J)}$ is dense and unstructured hence:

$$\mathcal{T} = \mathcal{O} \left(m \frac{d}{J} \right) = \mathcal{O} \left(\frac{s}{J} \log(d/J) \frac{d}{J} \right) = \tilde{\mathcal{O}} \left(\frac{sd}{J^2} \right).$$

As noted in [22], n may be taken to be $\mathcal{O}(1)$ (In all our experiments we take $n \leq 10$). For ZO-BCD-RC, as Z is a partial circulant matrix, we may exploit a fast matrix-vector multiplication via fast Fourier transform to reduce the complexity to $\mathcal{O}(d/J \log(d/J)) = \tilde{\mathcal{O}}(d/J)$.

Finally, we note that for both variants the memory complexity of ZO-BCD is dominated by the cost of storing Z . Again, as Z is dense and unstructured in ZO-BCD-R there are no tricks that one can exploit here, so the storage cost is $m(d/J) = \tilde{\mathcal{O}}(sd/J^2)$. For ZO-BCD-RC, instead of storing the entire partial circulant matrix Z , one just needs to store the generating vector $z \in \mathbb{R}^{d/J}$ and the index set Ω . Assuming we are allocating 32 bits per integer, this requires:

$$\frac{d}{J} + 32 \cdot b_3 \frac{s}{J} \log^2 \left(\frac{s}{J} \right) \log^2 \left(\frac{d}{J} \right) = \mathcal{O} \left(\frac{d}{J} \right).$$

This finishes the proof. \square

D Experimental setup details

In this section, we provide the detailed experimental settings for the numerical results provided in Section 5. Furthermore, we implemented a Python version and a Matlab version of ZO-BCD, and both implementations can be find online at <https://github.com/YuchenLou/ZO-BCD>.

D.1 Settings for synthetic experiments

For both synthetic examples, we use problem dimension $d = 20,000$ and gradient sparsity $s = 200$. Moreover, we use additive Gaussian noise with variance $\sigma = 10^{-3}$ in the oracles. The sampling radius is chosen to be 10^{-2} for all tested algorithms. For ZO-BCD, we use 5 blocks with uniform step size⁷ $\alpha = 0.9$, and the per block sparsity is set to be $s_{\text{block}} = 1.05s/J = 42$. Furthermore, the block gradient estimation step runs at most $n = 10$ iterations of CoSaMP. For the other tested algorithms, we hand tune the parameters for their best performance, and same step sizes are used when applicable. Note that SPSA must use a very small step size ($\alpha = 0.01$) in max- s -squared-sum problem, or it will diverge.

Re-shuffling the blocks. Note that the max- s -squared-sum function does not satisfy the Lipschitz differentiability condition (*i.e.* Assumption 1). Moreover the gradient support changes, making this an extremely difficult zeroth-order problem. To overcome the difficulty of discontinuous gradients, we apply an additional step that re-shuffles the blocks every J iterations. This re-shuffling trick is not required for the problems that satisfies our assumptions; nevertheless, we observe very similar convergence behavior with slightly more queries when the re-shuffling step was applied on the problems that satisfy the aforementioned assumptions.

D.2 Settings for sparse DWT attacks on images

We allow a total query budget of 10,000 for all tested algorithms in each image attack, *i.e.* an attack is considered a failure if it cannot change the label within 10,000 queries. We use a 3-level ‘db45’ wavelet transform. All the results present in Section 5.2 use the half-point symmetric boundary extension, hence the wavelet domain has a dimension of 676,353; slightly larger than the original pixel domain dimension. For the interested reader, a discussion and more results about other boundary extensions can be found in Appendix E.

For all variations of ZO-BCD, we choose the block size to be 170 with per block sparsity $s_{\text{block}} = 10$, thus $m = 52$ queries are used per iteration. Sampling radius is set to be 10^{-2} . The block gradient estimation step runs at most $n = 30$ CoSaMP iterations, and step size $\alpha = 10$.

⁷We note that using a line search for each block would maximize the advantage of block coordinate descent algorithms such as ZO-BCD, but we did not do so here for fairness

D.3 Settings for sparse CWT attacks on audio signals

For both targeted and untargeted CWT attack, we use Morse wavelets with 111 frequencies, which significantly enlarges the problem dimension from 16,000 to 1,776,000 per clip. In the attack, we choose the block size to be 295 with per block sparsity $s_{\text{block}} = 9$, thus $m = 52$ queries are used per iteration. The sampling radius is $\delta = 10^{-3}$. The block gradient estimation step runs at most $n = 30$ CoSaMP iterations. In targeted attacks, the step size is $\alpha = 0.05$, and Table 3 specifies the step size used in untargeted attacks.

In Table 3, we also include the results of a time domain attack for comparison. The parameter settings are the same as the aforementioned untargeted CWT attack settings, but we have to reduce the step size to 0.01 for stability. Also, note that the problem domain is much smaller in the original voice domain, so the number of blocks is much less while we keep the same block size.

E More experimental results and discussion

E.1 Sparse DWT attacks on images

Periodic extension. As mentioned, when we use boundary extensions other than periodic extension, the dimension of the wavelet coefficients will increase, depending on the size of wavelet filters and the level of the wavelet transform. More precisely, wavelets with larger support and/or deeper levels of DWT result in a larger increase in dimensionality. On the other hand, using periodic extension will not increase the dimension of wavelet domain. We provide test results for both boundary extensions in this section for the interested reader.

Compressed attack. As discussed in Section 4, DWT is widely used in data compression, such as JPEG-2000 for image. In reality, the compressed data are often saved in the form of sparse (and larger) DWT coefficients after vanishing the smaller ones. While we have already tested an attack on the larger DWT coefficients only (see Section 5.2), it is also of interest to test an attack after compression. That is, we zero out the smaller wavelet coefficients ($\text{abs} \leq 0.05$) first, and then attack on only the remaining, larger coefficients.

We use the aforementioned parameter settings for these two new attacks. We present the results in Table 4, and for completeness we also include the results already presented in Table 1. One can see that ZO-BCD-R(compressed) has higher attack success rate and lower ℓ_2 distortion, exceeding the prior state-of-the-art as presented in Table 1. We caution that this is not exactly a fair comparison with prior works however, as the compression step modifies the image before the attack begins.

Defense tests. Finally, we also tested some simple mechanisms for defending against our attacks; specifically harmonic denoising. We test DWT with the famous Haar wavelets,

Table 4: Results of untargeted image adversarial attack using various algorithms. Attack success rate (ASR), average final ℓ_2 distortion, and number of queries till first successful attack. ZO-BCD-R(periodic ext.) stands for ZO-BCD-R applying periodic extension for implementing the wavelet transform. ZO-BCD-R(compressed) stands for applying ZO-BCD-R to attack only large wavelet coefficients ($\text{abs} \geq 0.05$) and vanishing the smaller values. The other methods are the same in Table 1.

METHODS	ASR	ℓ_2 DIST	QUERIES
ZO-SCD	78%	57.5	2400
ZO-SGD	78%	37.9	1590
ZO-AdaMM	81%	28.2	1720
ZORO	90%	21.1	2950
ZO-BCD-R	92%	14.1	2131
ZO-BCD-RC	92%	14.2	2090
ZO-BCD-R(periodic ext.)	95%	21.0	1677
ZO-BCD-R(compressed)	96%	13.1	1546
ZO-BCD-R(large coeff.)	96%	13.7	1662

DWT with db45 wavelets which is also used for attack, and the essential discrete cosine transform (DCT). The defense mechanism is to apply the transform to the attacked images and then denoise by zeroing out small wavelet coefficients before transforming back to the pixel domain. We only test the defense on images that were successfully attacked. Tables 5 and 6 show the results of defending against the ZO-BCD-R and ZO-BCD-R(large coeff.) attacks respectively. Interestingly, using the attack wavelet (*i.e.* db45) in defence is not a good strategy. We obtain the best defense results by using a mismatched transform (*i.e.* DCT or Haar defense for a db45 attack) and a small thresholding value.

Table 5: Defense of image adversarial wavelet attack by ZO-BCD-R. Defense recovery success rate under haar and db45 wavelet filters, and discrete cosine transform (DCT) filter. Thresholding values of 0.05, 0.10, 0.15, and 0.20 were considered.

DEFENCE METHODS	0.05	0.10	0.15	0.20
Haar	74%	75%	76%	75%
db45	74%	72%	71%	63%
DCT	72%	79%	75%	67%

Table 6: Defense of image adversarial wavelet attack by ZO-BCD-R (large coeff.). Defense recovery success rate under Haar and db45 wavelet filters, and discrete cosine transform (DCT) filter. Thresholding values 0.05, 0.10, 0.15, and 0.20 were considered.

DEFENCE METHODS	0.05	0.10	0.15	0.20
Haar	75%	72%	78%	76%
db45	71%	70%	69%	63%
DCT	62%	74%	68%	58%

More adversarial examples. In Figure 4, we presented some adversarial images generated by the ZO-BCD-R and ZO-BCD-R(large coeff.) attacks. For the interested reader, we present more visual examples in Figure 6, and include the adversarial attack results generated by all versions of ZO-BCD.

E.2 Sparse CWT attacks on audio signals

Adversarial attacks on speech recognition is a more nebulous concept than that of adversarial attacks on image classifiers, with researchers considering a wide variety of threat models. In [49], an attack on the speech-to-text engine DeepSpeech [50] is successfully conducted, although the proposed algorithm, Houdini, is only able to force minor mis-transcriptions (“A great saint, saint Francis Xavier” becomes “a green thanked saint fredstus savia”). In [44], this problem is revisited, and they are able to achieve 100% success in targeted attacks, with any initial and target transcription from the Mozilla Common Voices dataset (for example, “it was the best of times, it was the worst of times” becomes “it is a truth universally acknowledged that a single”). We emphasize that both of these attacks are *whitebox*, meaning that they require full knowledge of the victim model. We also note that speech-to-text transcription is not a classification problem, thus the classic Carlini-Wagner loss function so frequently used in generating adversarial examples for image classifiers cannot be straightforwardly applied. The difficulty of designing an appropriate attack loss function is discussed at length in [44].

A line of research more related to the current work is that of attacking keyword classifiers. Here, the victim model is a classifier; designed to take as input a short audio clip and to output probabilities of this clip containing one of a small, predetermined list of keywords (“stop”, “left” and so on). Most such works consider the `SpeechCommands` dataset [37]. To the best of the author’s knowledge, the first paper to consider targeted attacks on a keyword classification model was [10], and they do so in a black-box setting. They achieve an 87% attack success rate (ASR) using a genetic algorithm, whose query complexity is unclear. They do not report the relative loudness of their attacks; instead they report the results of a

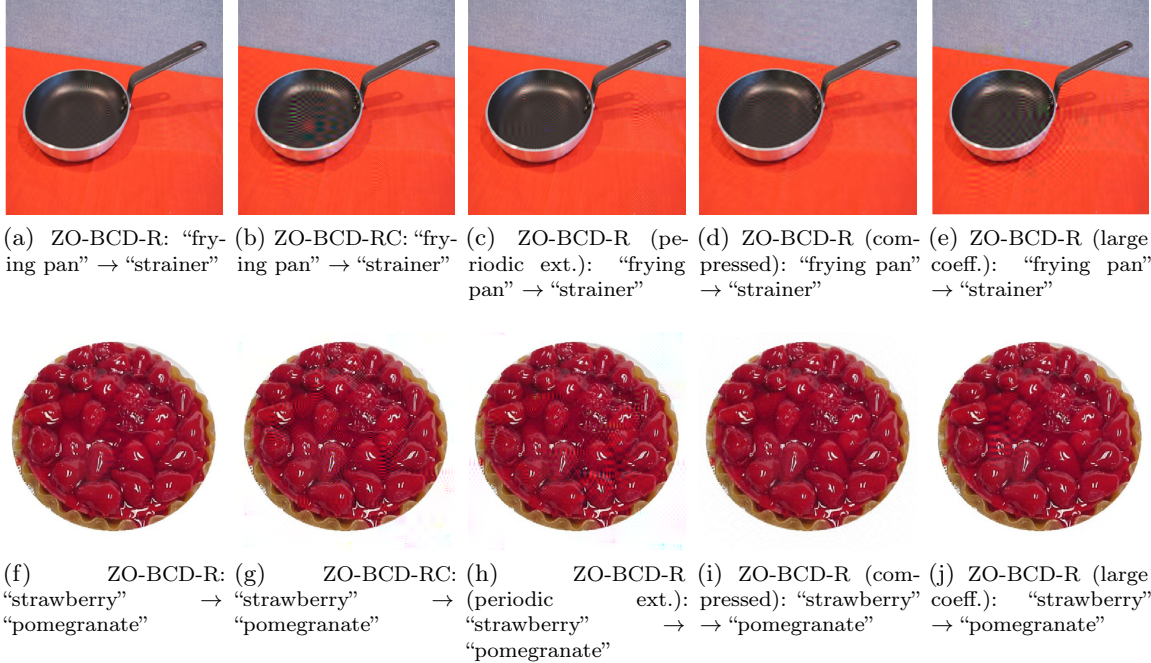


Figure 6: More examples of wavelet attacked images by ZO-BCD-R, ZO-BCD-RC, ZO-BCD-R(periodic ext.), ZO-BCD-R(compressed), and ZO-BCD-R(large coeff.), with true labels and mis-classified labels.

human study in which they asked volunteers to listen to and label the attacked audio clips. They report that for 89% of the successfully attacked clips human volunteers still assigned the clips the correct (*i.e.* source) label, indicating that these clips were not corrupted beyond comprehension. Their attacks are per-clip, *i.e.* not universal.

In [38], universal and untargeted attacks on a `SpeechCommands` classifier are considered. Specifically, they seek to construct a distortion δ such that for *any* clip x from a specified source class (*e.g.* “left”), the attacked clip $x + \delta$ is misclassified to a source class (*e.g.* “yes”) by the model. They consider several variations on this theme; allowing for multiple source classes. The results we recorded in Section 5.3 (ASR of 70.4% at a remarkably low mean relative loudness of -41.63 dB) were the best reported in the paper, and were for the single-source-class setting. This attack was in the white-box setting.

Finally, we mention two recent works which consider very interesting, but different threat models. [39] considers the situation where a malicious attacker wishes to craft a short (say half a second long) that can be added to *any* part of a clean audio clip to force a misclassification. Their attacks are targeted and universal, and conducted in the white-box setting. They do not report the relative loudness of their attacks. In [40], a generative model is trained that takes as input a benign audio clip x , and returns an attacked clip

$x + \delta$. The primary advantage of this approach is that attacks can be constructed on the fly. In the targeted, per-clip white-box setting they achieve the success rate of 93.6% advertised in Section 5.3, at an approximate relative loudness of -30 dB. They also consider universal attacks, and a transfer attack whereby the generative model is trained on a surrogate classification model.

In all the aforementioned keyword attacks, the victim model is some variant of the model proposed in [42]. Specifically, the audio input is first transformed into a 2D spectrogram using Mel frequency coefficients, bark coefficients or similar. Then, a 3–5 layer convolutional neural network is applied.